

1 **TOPOGRAPHY OPTIMIZATION FOR ENHANCING MICROALGAL**  
2 **GROWTH IN RACEWAY PONDS\***

3 OLIVIER BERNARD <sup>†</sup>, LIU-DI LU <sup>‡</sup>, JACQUES SAINTE-MARIE <sup>§</sup>, AND JULIEN  
4 SALOMON<sup>§</sup>

5 **Abstract.** Modeling the evolution process for the growth of microalgae in an artificial pond  
6 is a huge challenge, given the complex interaction between hydrodynamics and biological processes  
7 occurring across various timescales. In this paper, we consider a raceway, i.e., an oval pond where  
8 the water is set in motion by a paddle wheel. Our aim is to investigate theoretically and numerically  
9 the impact of bottom topography in such raceway ponds on microalgae growth. To achieve this goal,  
10 we consider a biological model based on the Han model, coupled with the Saint–Venant systems that  
11 model the fluid. We then formulate an optimization problem, for which we apply the weak maximum  
12 principle to characterize optimal topographies that maximize biomass production over one lap of the  
13 raceway pond or multiple laps with a paddle wheel. In contrast to a widespread belief in the field  
14 of microalgae, we show that a flat topography in a periodic regime satisfies the necessary optimality  
15 condition, and observe in the numerical experiments that the flat topography is actually optimal  
16 in this case. However, non-trivial topographies may be more advantageous in alternative scenarios,  
17 such as when considering the effects of mixing devices within the model. This study sheds light  
18 on the intricate relationship between bottom topography, fluid dynamics, and microalgae growth in  
19 raceway ponds, offering valuable insights into optimizing biomass production.

20 **Key words.** optimal control, weak maximum principle, microalgae, Han model, Saint–Venant  
21 system, raceway pond, shape optimization

22 **1. Introduction.** The numerical design of microalgae production technologies  
23 has been for decades a source of many interesting challenges not only in engineering  
24 but also in the area of scientific computing [13, 24, 38, 21]. The potential of these  
25 emerging photosynthetic organisms is found in cosmetics, pharmaceutical fields, food,  
26 and - in the long term - in green chemistry and energy applications [37]. Outdoor  
27 production is mainly carried out in open bioreactors with a raceway shape. Algae  
28 grow while exposed to solar radiation in these circular basins, where the water is set  
29 in motion by a paddle wheel. This mixing device homogenizes the medium, ensures  
30 equidistribution of nutrients, and guarantees that each cell will have regular access to  
31 light [9, 12]. The algae are harvested periodically, and their concentration is main-  
32 tained around an optimal value [28, 31]. The penetration of light is strongly reduced  
33 by the algal biomass, and less than 1% of the incident light reaches the reactor bot-  
34 tom [6]. In the case of larger biomass, the light extinction is so high that a large  
35 fraction of the population evolves in the dark and does not grow anymore. At low  
36 biomass density, a fraction of the solar light is not used by the algae and the pro-  
37 ductivity is suboptimal. Theoretical work has determined the optimal biomass for  
38 maximizing productivity [23, 17, 2].

39 Here, we consider another approach which consists in improving the photopro-

---

\*Submitted to the editors DATE.

**Funding:** This work was funded by the ...

<sup>†</sup>INRIA Sophia Antipolis Méditerranée, BIOCORE Project-Team, Université Nice Côte d'Azur, 2004, Route des Lucioles - BP93, 06902 Sophia-Antipolis Cedex, France and Sorbonne Université, INSU-CNRS, Laboratoire d'Océanographie de Villefranche, 181 Chemin du Lazaret, 06230 Villefranche-sur-mer, France (olivier.bernard@inria.fr).

<sup>‡</sup>Section de Mathématiques, Université de Genève, rue du Conseil-Général 5-7, CP 64, 1205, Geneva, Switzerland (liudi.lu@unige.ch).

<sup>§</sup>INRIA Paris, ANGE Project-Team, 75589 Paris Cedex 12, France and Sorbonne Université, CNRS, Laboratoire Jacques-Louis Lions, 75005 Paris, France (jacques.sainte-marie@inria.fr, julien.salomon@inria.fr).

duction process by controlling the cell trajectories in the light field. We start from the observation that algal raceway ponds are dynamical systems combining a physical aspect - the hydrodynamical behavior of the fluid transporting the algae culture, and a biological aspect - the light harvesting by the chlorophyll complexes in the cells [1, 29, 30]. We then study the effect of topography (or bathymetry) on growth to optimize the light received by the microalgae. Modeling this system is challenging, since it also involves the free-surface incompressible Navier–Stokes system [7, 10, 36, 27]. The complexity of this model generally prevents obtaining explicit formulas, and large computational resources are required to perform simulations.

Several experimental campaigns [25, 32] have shown that in the straight sections of the raceway, the flow is not disturbed (which was further confirmed by CFD modelling [19, 20]). Therefore, in these regions, despite turbulent dispersion, mixing is relatively poor. This mixing is mainly induced locally by the paddle wheel and, to a lesser extent, by the bends. The recent study of [20] confirms this finding, i.e., the turbulence is mainly generated near the paddle wheel and close to the surface.

We therefore focus on the main part of the raceway, outside the paddle-wheel area, and assume laminar flux. We study how to improve productivity in this part by modifying the bottom topography. This enables us to discuss the common belief that some specific topographies can bring more light to the algae in lower parts of the raceway, since cells get closer to the surface when reaching peaks in these topographies.

Let us detail our approach. We first introduce a coupled model to represent the growth of algae in a one dimensional (1D) raceway pond, accounting for the light that they receive. This model is obtained by combining the Han photosynthesis equations with a hydrodynamic law based on the Saint–Venant system. This first step enables us to formulate an optimization problem in which the topography of the raceway is designed to maximize productivity. We then use an adjoint-based optimization scheme to include the constraints associated with the Saint–Venant regime. We prove that the flat topography satisfies the first-order optimality systems in a periodic case, focusing on the fraction of the raceway in laminar regime. However, non-trivial topographies can be obtained in other contexts, e.g., when the periodic assumption is removed or when the mixing device is accounted for in conjunction with the bottom topography. Numerical simulations show that a combination of turbulence-induced mixing and non-flat topographies can slightly increase biomass production. However, enhancing the turbulence by mixing significantly increases productivity and is definitely the most efficient approach [5, 4], even if more energy is dissipated in this process.

The outline of the paper is as follows. In Section 2, we present the biological and hydrodynamical models underlying our coupled system. In Section 3, we describe the optimization problem and a corresponding numerical optimization procedure. Section 4 is devoted to the numerical results obtained with our approach. We then conclude with some perspectives opened up by this work.

**2. Hydrodynamic and biological models.** Our approach is based on a coupling of the hydrodynamic transport of the particles with the photosystems evolution driven by the light intensity they receive when traveling in the raceway pond.

**2.1. Hydrodynamical model and Lagrangian trajectories.** Saint–Venant equations are a popular model of geophysical flows. This system is derived from the free surface incompressible Navier–Stokes equations (see, for instance, [15]). Here, we focus on its 1D smooth steady state solutions in a laminar regime, which satisfy

$$(2.1) \quad \partial_x(hu) = 0, \quad \partial_x(hu^2 + g\frac{h^2}{2}) = -gh\partial_x z_b,$$

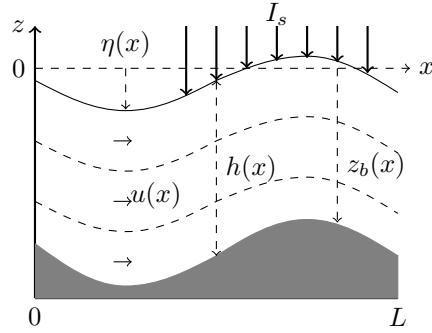


FIG. 1. Representation of the one dimensional hydrodynamic model.

88 where  $h$  is the water depth,  $u$  is the horizontal averaged velocity of the fluid, the  $g$   
 89 is the gravitational constant, and  $z_b$  is the topography. The free surface  $\eta$  and the  
 90 average discharge are given by  $\eta := h + z_b$  and  $Q = hu$  respectively. This system is  
 91 presented in Figure 1. The  $z$  (resp.  $x$ ) axis represents the vertical (resp. horizontal)  
 92 direction and  $I_s$  is the light intensity on the free surface (assumed to be constant).

93 Integrating the equation on the left of (2.1), we get

$$94 \quad (2.2) \quad hu = Q_0,$$

95 for a fixed positive constant  $Q_0$ . This implies a constant discharge in space. Then  
 96 the equation on the right-hand side of (2.1) can be rewritten by

$$97 \quad (2.3) \quad hu\partial_x u + h\partial_x gh + h\partial_x gz_b = 0.$$

98 Assume that  $h$  is non-zero, dividing then the equality (2.3) by  $h$  and using (2.2) to  
 99 eliminate  $u$ , we get  $\partial_x \left( \frac{Q_0^2}{2h^2} + g(h + z_b) \right) = 0$ . Given  $h(0), z_b(0) \in \mathbb{R}$ , we obtain

$$100 \quad \frac{Q_0^2}{2h(x)^2} + g(h(x) + z_b(x)) = \frac{Q_0^2}{2h^2(0)} + g(h(0) + z_b(0)) =: M_0,$$

101 which holds for all  $x \in [0, L]$ , meaning that the topography  $z_b$  satisfies

$$102 \quad (2.4) \quad z_b = \frac{M_0}{g} - \frac{Q_0^2}{2gh^2} - h.$$

103

104 *Remark 2.1.* Let  $Fr = \frac{u}{\sqrt{gh}}$  be the Froude number. The situation  $Fr < 1$  cor-  
 105 responds to the subcritical case (i.e., the flow regime is *fluvial*), while  $Fr > 1$  corre-  
 106 sponds to the supercritical case (i.e., the flow regime is *torrential*). In the steady case,  
 107 the threshold value  $h = h_c$  is obtained for  $Fr = 1$ ; using (2.2), we find  $h_c := \left(\frac{Q_0^2}{g}\right)^{\frac{1}{3}}$ .

108 Because of (2.4),  $h$  solves a third-order polynomial equation. Given a smooth topog-  
 109 raphy  $z_b$ , if  $h_c + z_b + \frac{Q_0^2}{2gh_c^2} - \frac{M_0}{g} < 0$ , there exists a unique positive smooth solution  
 110 of (2.4) that satisfies the subcritical flow condition (see [26, Lemma 1]).

111 From the incompressibility of the flow, we have  $\nabla \cdot \mathbf{u} = 0$  with  $\mathbf{u} = (u(x), w(x, z))$ .  
 112 Here,  $w(x, z)$  is the vertical velocity. Incompressibility implies  $\partial_x u + \partial_z w = 0$ . Inte-

113 grating the latter from the topography  $z_b$  to an arbitrary vertical position  $z$  gives:

$$\begin{aligned}
 0 &= \int_{z_b}^z (\partial_x u(x) + \partial_\xi w(x, \xi)) d\xi \\
 &= (z - z_b) \partial_x u(x) + w(x, z) - w(x, z_b) \\
 &= (z - z_b) \partial_x u(x) - u(x) \partial_x z_b + w(x, z) \\
 &= \partial_x ((z - z_b) u(x)) + w(x, z),
 \end{aligned}$$

115 where we have used the kinematic condition at the bottom, i.e.,  $w(x, z_b) = u(x) \partial_x z_b$ .  
 116 It follows from (2.4) that

$$(2.5) \quad w(x, z) = \left( \frac{M_0}{g} - \frac{3u^2(x)}{2g} - z \right) u'(x),$$

118 with  $u'(x)$  the derivative of  $u$  with respect to  $x$ .

119 Let the pair  $(x(t), z(t))$  be the position of a particle (or an algal cell) at time  $t$  in  
 120 the raceway pond. The Lagrangian trajectory is characterized by

$$(2.6) \quad \begin{pmatrix} \dot{x}(t) \\ \dot{z}(t) \end{pmatrix} = \begin{pmatrix} u(x(t)) \\ w(x(t), z(t)) \end{pmatrix},$$

122 with the initial position at time 0,  $(x(0), z(0)) = (x_0, z_0)$ .

123 *Remark 2.2.* The geometry of the raceway pond with small dissipation and shear  
 124 effects (reduced wall friction and viscosity) justifies a laminar flow modeled by a  
 125 shallow-water model, such as the Saint-Venant system. This regime also minimizes  
 126 the mixing energy and hence is favored at the industrial scale.

127 A higher mixing energy would lead to a turbulent regime. A possible way to enrich  
 128 the representation of Lagrangian trajectories in this case would consist in including  
 129 a Brownian into (2.6). However, getting time-free expressions of the trajectories (as  
 130 in (2.7) and (2.12)) in this case is much more challenging, so that such a strategy  
 131 would require a large set of simulations together with an averaging strategy.

132 The Lagrangian trajectory given by (2.6) is a general formulation, which still  
 133 holds when we change the hydrodynamical model. In our setting, we can find a time-  
 134 free formulation of the Lagrangian trajectory. More precisely, we denote by  $z(x)$  the  
 135 depth of a particle at position  $x$ . From (2.5) and (2.6), we get

$$(2.7) \quad z' := \frac{\dot{z}}{\dot{x}} = \left( \frac{M_0}{g} - \frac{3u^2}{2g} - z \right) \frac{u'}{u}.$$

137 From (2.2), (2.4) and the definition of the free surface  $\eta$ , we have

$$(2.8) \quad \eta = h + z_b = \frac{M_0}{g} - \frac{u^2}{2g},$$

139 which implies that  $\eta' = -uu'/g$ . Multiplying then (2.7) on both sides by  $u$ , and using  
 140 the formulation of  $\eta$  and  $\eta'$ , one finds

$$(2.9) \quad z'u + zu' = \left( \eta - \frac{u^2}{g} \right) u' = \eta u' + \eta' u,$$

142 which implies that  $(u(z - \eta))' = 0$ . Using again the identity (2.2), one obtains  
 143  $\eta(x) - z(x) = \frac{h(x)}{h(0)} (\eta(0) - z(0))$ . This equation shows that given the initial water

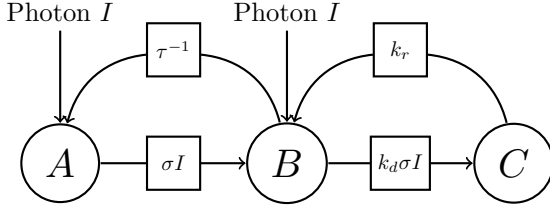


FIG. 2. Han's model, describing the state transition probability, as a function of the photon flux.

144 depth  $h(0)$  and the initial free surface position  $\eta(0)$ , the distance between a trajectory  
 145  $z$  (starting from the position  $z(0)$ ) and the free surface  $\eta$  depends only on the water  
 146 depth  $h$ . On the other hand, the time-free formulation of the trajectory reads

147 (2.8) 
$$z(x) = \eta(x) - \frac{h(x)}{h(0)}(\eta(0) - z(0)).$$

148 We will further exploit the property of this formulation in Section 3.

149 *Remark 2.3.* Since  $Q_0$  is chosen to be positive,  $h$  is necessarily positive. More-  
 150 over, if  $z(0)$  belongs to  $[z_b(0), \eta(0)]$ , then  $z(x)$  belongs to  $[z_b(x), \eta(x)]$ . In particular,  
 151 choosing  $z(0) = z_b(0)$  in (2.8) and using (2.2) give  $z(x) = z_b(x)$ . In the same way, we  
 152 find that  $z(x) = \eta(x)$  when  $z(0) = \eta(0)$ .

153 **2.2. Modelling the dynamics of the photosystems.** To describe the dy-  
 154 namics of photosystems, we use here the Han model [18]. This model is generally  
 155 considered to characterize the photosynthetic process of these subunits as they har-  
 156 vest photons and transfer their energy to the cell to fix  $\text{CO}_2$ .

157 **2.2.1. The Han model.** The Han model is a compartmental model in which  
 158 the photosystems are described by three different states: open and ready to harvest a  
 159 photon ( $A$ ), closed while processing the absorbed photon energy ( $B$ ), or inhibited if  
 160 several photons have been absorbed simultaneously ( $C$ ). The relation of these three  
 161 states are schematically presented in Fig. 2.

162 The evolution satisfies the following ordinary differential equations (ODEs)

163 (2.9) 
$$\begin{aligned} \dot{A} &= -\sigma IA + \frac{B}{\tau}, \\ \dot{B} &= \sigma IA - \frac{B}{\tau} + k_r C - k_d \sigma IB, \\ \dot{C} &= -k_r C + k_d \sigma IB. \end{aligned}$$

164 Here,  $I$  denotes the light density, a continuous time-varying signal. The states  $A$ ,  $B$ ,  
 165 and  $C$  are the relative frequencies of three possible states with  $A + B + C = 1$ , so  
 166 that (2.9) can be reduced to a system in dimension two by eliminating the state  $B$ .  
 167 Here,  $\sigma$  stands for the specific photon absorption,  $\tau$  is the turnover rate,  $k_r$  and  $k_d$   
 168 represent the photosystem repair and the damage rates, which are all positive.

169 The dynamics of the open state  $A$  can be shown to be much faster than the  
 170 dynamics of the photoinhibition state  $C$ . A slow-fast approximation by using singular  
 171 perturbation theory (as shown in details in [21]) leads to the simplification of the  
 172 dynamics driven by the slow dynamics of  $C$ :

173 (2.10) 
$$\dot{C} = -\alpha(I)C + \beta(I),$$

174 where

$$175 \quad (2.11) \quad \alpha(I) = k_d \tau \frac{(\sigma I)^2}{\tau \sigma I + 1} + k_r, \quad \beta(I) = k_d \tau \frac{(\sigma I)^2}{\tau \sigma I + 1}.$$

176 Repeating the reasoning done to get (2.7) with (2.10) and (2.2), we can also find a  
177 time-free reformulation, namely

$$178 \quad (2.12) \quad C' := \frac{\dot{C}}{\dot{x}} = \frac{-\alpha(I)C + \beta(I)}{Q_0} h,$$

179 where all the functions on the right-hand side only depend on the spatial variable  $x$ .

180 **2.2.2. Periodic setting.** We consider the case where  $C$  is periodic, with a pe-  
181 riod corresponding to one lap of the raceway pond. This situation occurs, e.g., when  
182 an appropriate harvest is performed after each lap. To describe the corresponding  
183 model, we first consider a variant of the usual Cauchy problem (2.12):

184 *Given  $I \in \mathcal{C}([0, L]; \mathbb{R})$ ,  $I \geq 0$ , find  $(C_0, C) \in [0, 1] \times \mathcal{C}([0, L]; [0, 1])$  such that*

$$185 \quad (2.13) \quad \begin{cases} C'(x) = \frac{-\alpha(I(x))C(x) + \beta(I(x))}{Q_0} h(x), & x \in [0, L], \\ C(L) = C(0) = C_0. \end{cases}$$

186 Let us show that the solution  $C(x)$  of (2.13) exists. Indeed, applying the Duhamel's  
187 formula on the Cauchy problem associated with (2.12) and the initial condition  $C(0) =$   
188  $C_0$ , and using the inequality  $\beta(I) \leq \alpha(I)$  gives

$$189 \quad \begin{aligned} C(L) - C_0 &= - \left( 1 - e^{-\int_0^L \frac{\alpha(I(s))h(s)}{Q_0} ds} \right) C_0 + \int_0^L e^{-\int_s^L \frac{\alpha(I(y))h(y)}{Q_0} dy} \frac{\beta(I(s))h(s)}{Q_0} ds \\ &\leq \left( 1 - e^{-\int_0^L \frac{\alpha(I(s))h(s)}{Q_0} ds} \right) (1 - C_0). \end{aligned}$$

190 Hence the affine mapping  $\Phi : C_0 \mapsto C(L) - C_0$  satisfies  $\Phi(0) \geq 0$ , and the inequality  
191 implies that  $\Phi(1) \leq 0$ . It follows that there exists a unique  $C_0 \in [0, 1]$  that satisfies  
192  $C(L) - C_0 = 0$ . Using *Intermediate Value Theorem*, we get the next result.

193 **THEOREM 2.4.** *There exists a unique couple  $(C_0, C) \in [0, 1] \times \mathcal{C}([0, L]; [0, 1])$  that*  
194 *satisfies (2.13).*

195 **2.2.3. Growth rate.** Finally, the net growth rate of the photosystem is defined  
196 by balancing photosynthesis and respiration, which gives

$$197 \quad (2.14) \quad \mu(C, I) := \zeta(I) - \gamma(I)C,$$

198 where

$$199 \quad (2.15) \quad \gamma(I) = \frac{k\sigma I}{\tau\sigma I + 1}, \quad \zeta(I) = \frac{k\sigma I}{\tau\sigma I + 1} - R.$$

200 Here,  $k$  is a factor that relates the received energy with the growth rate and  $R$  repre-  
201 sents the respiration rate.

202 **2.3. Coupling of two systems.** As shown in the previous section, the light  
 203 intensity  $I$  plays an important role in algal growth, since it triggers photosynthesis.  
 204 On the other hand, the position of the algae influences the light perceived as well as  
 205 the efficiency of the photosynthesis process. Therefore, the light intensity is the main  
 206 connection which couples the hydrodynamic model and the physiological evolution of  
 207 the algae. To evaluate the light intensity observed on the trajectory  $z$ , we assume that  
 208 the growth process occurs at a much slower timescale than that of hydrodynamics and  
 209 is, as such, negligible for one lap over the raceway. In the same way, uncertainties  
 210 such as rainfall and evaporation, can also be neglected at this timescale. These fac-  
 211 tors can be taken into account for longer timescale using more detailed models, see for  
 212 instance [11, 8]. In this framework, the Beer–Lambert law describes how light is atten-  
 213 uated with depth  $\xi$  by  $I(x, \xi) := I_s \exp(-\varepsilon(\eta(x) - \xi))$ , where  $\varepsilon$  is the light extinction  
 214 coefficient. Replacing  $\xi$  in the previous formulation by the trajectory (2.8), we then  
 215 get the following expression for the captured light intensity along the trajectory  $z(x)$ :

$$216 \quad (2.16) \quad I(x, z(x)) = I_s \exp\left(-\varepsilon \frac{h(x)}{h(0)}(\eta(0) - z(0))\right).$$

217 In particular, we observe that for given data  $I_s$ ,  $\varepsilon$ ,  $h(0)$ , and  $\eta(0)$ , the perceived light  
 218 intensity along the trajectory  $z(x)$  only depends on its initial position  $z(0)$  and  $h(x)$ .

219 In order to evaluate the quality of this coupled system, we define the average net  
 220 growth rate of the system by

$$221 \quad (2.17) \quad \bar{\mu} := \frac{1}{V} \int_0^L \int_{z_b(x)}^{\eta(x)} \mu(C(x, z), I(x, z)) \, dz dx,$$

222 where  $\mu$  is defined by (2.14) and  $V := \int_0^L h(x) dx$  is the volume of our 1D raceway.

223 **3. Optimal control problem.** In this section, we define the optimal control  
 224 problems associated with our biological–hydrodynamic model. Depending on  $V$ , we  
 225 divide our study into two cases.

226 **3.1. Objective function and vertical discretization.** Our goal is to find  
 227 the optimal topography  $z_b$  that maximizes the average net growth rate (2.17). In  
 228 order to tackle numerically this optimization problem, let us first consider a vertical  
 229 discretization. Let  $N_z$  denotes the number of trajectories, we consider a uniform  
 230 vertical discretization of their initial position:

$$231 \quad (3.1) \quad z_i(0) := \eta(0) - \frac{i - \frac{1}{2}}{N_z} h(0), \quad i = 1, \dots, N_z.$$

232 Using the formulation (2.8), we find the trajectories  $z_i(x) := \eta(x) - \frac{i - \frac{1}{2}}{N_z} h(x)$ ,  $i =$   
 233  $1, \dots, N_z$ . In particular, the distribution of trajectories  $z_i(x)$  remains uniform along  
 234 the direction of  $x$ . Using (??), we obtain the perceived light intensity on  $z_i(x)$ :

$$235 \quad (3.2) \quad I(x, z_i(x)) = I_s \exp\left(-\varepsilon \frac{h(x)}{h(0)}(\eta(0) - z_i(0))\right) = I_s \exp\left(-\varepsilon \frac{i - \frac{1}{2}}{N_z} h(x)\right),$$

236 where we use the closed form of the light intensity (2.16) and the definition of  $z_i(0)$ .  
 237 To simplify notations and emphasis the dependence on the water depth  $h$ , we write  
 238  $I_i(h(x))$  instead of  $I(x, z_i(x))$  hereafter. The photoinhibition state  $C_i$  is then com-  
 239 puted using the evolution (2.12) for  $I = I_i(h)$ . In this setting, the semi-discrete

240 average net growth rate in the raceway pond can be derived from (2.17) as

$$241 \quad (3.3) \quad \bar{\mu}_{N_z}(h) := \frac{1}{VN_z} \sum_{i=1}^{N_z} \int_0^L \mu(C_i(x), I_i(h(x))) h(x) dx,$$

242 where  $h$  is the variable of the objective function, and  $\mu$  is given by (2.14). From now  
243 on, we focus on the subcritical case, i.e.,  $Fr < 1$ , see Remark 2.1. As mentioned  
244 in Section 2.1, in this regime, a given topography  $z_b$  corresponds to a unique water  
245 depth  $h$  which verifies this assumption.

246 *Remark 3.1.* Given a topography  $z_b$ , usual shallow-water solvers typically con-  
247 sider equations of type (2.4) to compute  $h$  in the simulations. Here, we use this  
248 equation in the opposite way, i.e., to recover  $z_b$  from  $h$ . In this way, we directly opti-  
249 mize  $h$  instead of  $z_b$ , since the expressions of the evolution of the state  $C$  (2.12), the  
250 light intensity (3.2) and the objective function (3.3) depend on  $h$  and not on  $z_b$ .

251 **3.2. Constant Volume.** For simplicity, we omit from now on the variable  $x$  in  
252 the notation and consider  $h$  as the variable of the light intensities  $(I_i)_{i=1, \dots, N_z}$  and  
253  $\bar{\mu}_{N_z}$ . For a fixed volume  $V > 0$  and a discharge  $Q_0 > 0$ , we seek an admissible controls  
254  $h \in L^\infty([0, L]; \mathbb{R})$ ,  $h > 0$  over a fixed length  $L > 0$ , that maximize the semi-discrete  
255 average net growth rate (3.3). Thus, the optimal control problem (OCP) reads

$$256 \quad (P1) \quad \begin{aligned} \max_{h \in L^\infty([0, L]; \mathbb{R}), h > 0} \bar{\mu}_{N_z}(h) &= \sum_{i=1}^{N_z} \int_0^L \frac{\mu(C_i(x), I_i(h(x)))}{VN_z} h(x) dx, \\ \text{s.t. } C_i' &= \frac{\beta(I_i(h)) - \alpha(I_i(h)) C_i}{Q_0} h, \\ C_i(0) &= C_i(L), \quad \forall i = 1, \dots, N_z, \\ v' &= h, \\ v(0) &= 0, \quad v(L) = V. \end{aligned}$$

257 Here, we use formula (2.14) for  $\mu$ ,  $h$  is the control variable, and  $(C_i, v)$  are the state  
258 variables, where  $v$  has been introduced to take into account the constraint  $V = hL$ .  
259 The Hamiltonian associated with (P1) is given by

$$260 \quad \begin{aligned} H(C_i, v, p_{C_i}, p_v, p_0, h) &= \sum_{i=1}^{N_z} p_{C_i} \frac{\beta(I_i(h)) - \alpha(I_i(h)) C_i}{Q_0} h \\ &+ p_v h + p_0 \sum_{i=1}^{N_z} \frac{\zeta(I_i(h)) - \gamma(I_i(h)) C_i \mu(C_i, I_i(h))}{VN_z} h, \end{aligned}$$

261 where  $(p_{C_i}, p_v)$  are the co-states of  $(C_i, v)$  respectively, and  $p_0$  is a real number. Sup-  
262 pose that  $h^* \in L^\infty([0, L]; \mathbb{R})$ ,  $h > 0$  is a maximizer, and  $C_i^*$ ,  $v^*$  are the corresponding  
263 solutions of the problem (P1). Using the weak maximum principle [35, Pages 33–  
264 35], there exist absolutely continuous functions  $p_{C_i}^* : [0, L] \rightarrow \mathbb{R}$ ,  $p_v^* : [0, L] \rightarrow \mathbb{R}$   
265 and a real number  $p_0^* \leq 0$ , such that for almost every  $x \in [0, L]$ , the extremals

266  $(C_i^*, v^*, p_{C_i}^*, p_v^*, p_0^*, h^*)$  satisfy the optimality system  
 (3.4)

$$\begin{aligned} C_i' &= \frac{\partial H}{\partial p_{C_i}} = \frac{\beta(I_i(h)) - \alpha(I_i(h)) C_i}{Q_0} h, \quad v' = \frac{\partial H}{\partial p_v} = h, \\ p_{C_i}' &= -\frac{\partial H}{\partial C_i} = p_{C_i} \frac{\alpha(I_i(h))}{Q_0} h + p_0 \frac{\gamma(I_i(h))}{VN_z} h, \quad p_v' = -\frac{\partial H}{\partial v} = 0, \\ 0 &= \frac{\partial H}{\partial h} = \sum_{i=1}^{N_z} p_{C_i} \frac{\beta'(I_i(h)) - \alpha'(I_i(h)) C_i}{Q_0} I_i'(h) h + \sum_{i=1}^{N_z} p_{C_i} \frac{\beta(I_i(h)) - \alpha(I_i(h)) C_i}{Q_0} \\ &\quad + p_0 \sum_{i=1}^{N_z} \frac{\zeta'(I_i(h)) - \gamma'(I_i(h)) C_i}{VN_z} I_i'(h) h + p_0 \sum_{i=1}^{N_z} \frac{\zeta(I_i(h)) - \gamma(I_i(h)) C_i}{VN_z} + p_v. \end{aligned}$$

268 LEMMA 3.2. *The extremal  $(C_i^*, v^*, p_{C_i}^*, p_v^*, p_0^*, h^*)$  which satisfies (3.4) is normal.*

269 *Proof.* We use the equivalent dual form of the Mangasarian-Fromovitz constraint  
 270 qualification [33, p. 255–269], i.e., we prove that if  $p_0^* = 0$ , then  $p_{C_i}^*$  and  $p_v^*$  are equal  
 271 to zero on  $[0, L]$ .

272 Substituting  $p_0^* = 0$  into (3.4), the ODE associated with  $p_{C_i}^*$  then reads

$$273 \quad (p_{C_i}^*)' = p_{C_i}^* \frac{\alpha(I_i(h^*))}{Q_0} h^*, \quad p_{C_i}^*(0) = p_{C_i}^*(L), \quad \forall i = 1, \dots, N_z,$$

274 where we complete by the periodic condition determined using  $C_i^*(0) = C_i^*(L)$ ,  
 275  $\forall i = 1, \dots, N_z$ . Note that  $Q_0 > 0$  and  $\alpha$  is a positive function from (2.11), and  
 276  $h^* > 0$ . Hence, we have  $\frac{\alpha(I_i(h^*))}{Q_0} h^* > 0$ . Using then a similar reasoning as for the  
 277 system (2.13), we find that the only solution of (3.5) is  $p_{C_i}^* = 0$ . Substituting  $p_{C_i}^* = 0$   
 278 and  $p_0^* = 0$  into the last equation of (3.4), we obtain  $p_v^* = 0$ , which contradicts the  
 279 fact that  $p_{C_i}^*$  and  $p_v^*$  are not identically 0 on  $[0, L]$ . Therefore,  $p_0^* < 0$ .  $\square$

280 When the extremal is normal,  $p_{C_i}^*$  and  $p_v^*$  are usually normalized so that  $p_0^* = -1$   
 281 what we set hereafter. Let us show that the flat topography satisfies (3.4).

282 THEOREM 3.3. *There exists  $p_v^f \in \mathbb{R}$  such that the constant water depth*

$$283 \quad h^f := \frac{V}{L},$$

284 *and the corresponding solutions  $(C_i^f)_{i=1, \dots, N_z}, (p_{C_i}^f)_{i=1, \dots, N_z}, v^f$  satisfy (3.4).*

285 *Proof.* From  $v' = h^f$  with  $v(0) = 0$ ,  $v(L) = V$ , we find  $v^f = \frac{V}{L}x$ . Given  $i \in$   
 286  $\{1, \dots, N_z\}$ , from (3.2), we deduce that

$$287 \quad I_i(h^f) = I_s \exp\left(-\varepsilon \frac{i - \frac{1}{2}}{N_z} h^f\right), \quad I_i'(h^f) = -\varepsilon \frac{i - \frac{1}{2}}{N_z} I_i(h^f),$$

288 which are constant on  $[0, L]$ . Solving the equation of  $C_i$  in (3.4) gives

$$289 \quad (3.6) \quad C_i(x) = e^{-\frac{\alpha(I_i(h^f))}{Q_0} h^f x} C_i(0) + \frac{\beta(I_i(h^f))}{\alpha(I_i(h^f))} (1 - e^{-\frac{\alpha(I_i(h^f))}{Q_0} h^f x}).$$

290 Since  $C_i$  is periodic (i.e.,  $C_i(L) = C_i(0)$ ), we get from the previous equation that  
 291  $C_i(0) = \frac{\beta(I_i(h^f))}{\alpha(I_i(h^f))}$ . Inserting this value in (3.6), we find

$$292 \quad C_i(x) = C_i^f := \frac{\beta(I_i(h^f))}{\alpha(I_i(h^f))}, \quad \forall x \in [0, L].$$

293 A similar reasoning applied to  $p_{C_i}$  gives  $p_{C_i}(x) = p_{C_i}^f = \frac{Q_0 \gamma(I_i(h^f))}{V N_z \alpha(I_i(h^f))}$ ,  $\forall x \in [0, L]$ .  
 294 It follows that all the terms in the sums of the last equation in (3.4) are constant  
 295 on  $[0, L]$ . Hence, there exists a  $p_v^f \in \mathbb{R}$  such that the extremal  $(C_i^f, v^f, p_{C_i}^f, p_v^f, h^f)$   
 296 satisfies the optimality system (3.4).  $\square$

297 *Remark 3.4.* The previous theorem shows that the flat topography satisfies the  
 298 necessary conditions of optimality. One can explore further second-order conditions  
 299 to check whether the flat topography is a local maximizer. However, the sign of the  
 300 eigenvalues of the Hessian operator of the average growth rate  $\text{Hess}(\bar{\mu}_{N_z})$  is in general  
 301 not constant with respect to a flat topography  $h^f = V/L$  and is rather difficult to  
 302 determine (see Appendix B).

303 Numerically, we observe that the flat topography is actually optimal in the peri-  
 304 odic case for standard values of the parameters (see Subsection 4.3.4).

305 *Remark 3.5.* If  $C$  is defined by a Cauchy problem and is not assumed to be  
 306 periodic (i.e.,  $C(0)$  is not necessarily equal to  $C(L)$ ), then (3.6) implies that  $C$  may  
 307 depend on  $x$  and the computations in the proof above no longer hold. In other words,  
 308 the flat topography is not necessarily an optimum in a non-periodic setting, which is  
 309 confirmed by our numerical tests (see Subsection 4.3.2).

### 310 3.3. Non-constant volume problem for maximizing areal productivity.

311 In the general case, the volume of the system  $V$  can also vary, hence can be optimized.  
 312 We now assume that the water depth is of the form  $h + h_0$ , where  $h \in L^\infty([0, L]; \mathbb{R})$   
 313 with  $h > -h_0$ ,  $\int_0^L h \, dx = 0$ , and  $h_0 > 0$  so that  $V = h_0 L$ . Here,  $V$  depends only on  
 314 the parameter  $h_0$ , as the length  $L > 0$  is fixed. Moreover, we have  $\frac{1}{L} \int_0^L h + h_0 \, dx =$   
 315  $\frac{0 + h_0 L}{L} = h_0$ , meaning that  $h_0$  represents the average depth of the system.

316 On the other hand, when  $V$  changes, the biomass concentration  $X$  (defined by  
 317  $\dot{X} = (\bar{\mu} - D)X$  with  $D$  the dilution rate) also changes. In this case, the light extinction  
 318  $\varepsilon$  in (2.16) can no longer be assumed to be constant. More precisely, we consider here

$$319 \quad (3.7) \quad \varepsilon(X) := \varepsilon_0 X + \varepsilon_1,$$

320 where  $\varepsilon_0 > 0$  is the specific light extinction coefficient of the microalgae species and  
 321  $\varepsilon_1 > 0$  stands for the background turbidity that summarizes the light absorption and  
 322 diffusion caused by all non-microalgae components [22].

323 To take into account the variation in  $X$  with respect to  $V$ , we also need to adapt  
 324 our objective function. More precisely, instead of considering the average net growth  
 325 rate  $\bar{\mu}$ , we maximize the areal productivity  $\Pi$ . Given a biomass concentration  $X$ , this  
 326 quantity is defined by

$$327 \quad (3.8) \quad \Pi := \bar{\mu} X \frac{V}{S},$$

328 where  $\bar{\mu}$  is the average net growth rate defined in (2.17) and  $S$  is the ground surface  
 329 of the raceway system which in our 1D system, actually means  $S = L$ .

330 Before stating the associated optimal control problem, we detail the relation be-  
 331 tween  $X$  and  $V$ . A standard criterion to determine this relation (see [23, 17]) consists  
 332 in regulating  $X$ , such that the steady state value of the net growth rate  $\mu_s$  at the  
 333 average depth  $h_0$  is 0, i.e.,

$$334 \quad (3.9) \quad \mu_s(I(h_0)) = 0, \quad \text{with} \quad \mu_s(I) := -\gamma(I) \frac{\beta(I)}{\alpha(I)} + \zeta(I).$$

335 Using the definitions (2.11), (2.15) for  $\alpha$ ,  $\beta$ ,  $\zeta$  and  $\gamma$ , one can solve (3.9) analytically,  
 336 and find that  $I(h_0)$  is one of the two roots, denoted by  $I_-$  and  $I_+$ , of the second order  
 337 polynomial equation  $k_d\tau R(\sigma I)^2 + (k_r\tau\sigma R - k_r k\sigma)I + k_r R = 0$ . In practice,  $I_-$ ,  $I_+$   
 338 are two real roots with  $I_- \leq I_+$ , and  $\mu_s(I) \geq 0$  on the interval  $[I_-, I_+]$ . Then, the  
 339 biomass concentration  $X$  in a given volume  $V$  is adjusted to get  $I(h_0) = I_-$ . More  
 340 precisely, using (2.16) with  $I(x, z) = I_-$ , we get

$$341 \quad (3.10) \quad X(h_0) = \frac{1}{\varepsilon_0} \left( \frac{Y_{\text{opt}}}{h_0} - \varepsilon_1 \right), \quad \text{with} \quad Y_{\text{opt}} := \ln \left( \frac{I_s}{I_-} \right).$$

342 Here,  $X$  is function of  $h_0$ , meaning that we can use the average depth  $h_0$  to control  
 343 both  $V$  and  $X$  in the non-constant volume case.

344 *Remark 3.6.* In bioengineering, the assumption (3.9) is usually called the *com-*  
 345 *ensation condition*, which describes the situation where the growth at the bottom  
 346 compensates exactly for the respiration. We refer to [2] for a detailed analysis.

347 We keep using a uniform vertical discretization, as in Section 3.1, but now  $z_i(0) :=$   
 348  $\eta(0) - \frac{i-\frac{1}{2}}{N_z}(h_0 + h(0))$ ,  $i = 1, \dots, N_z$ . Then the growth rate  $\bar{\mu}_{N_z}$  becomes

$$349 \quad (3.11) \quad \bar{\mu}_{N_z}(h, h_0) := \sum_{i=1}^{N_z} \int_0^L \frac{\mu(C_i(x), I_i(h_0 + h(x)))}{h_0 L N_z} (h_0 + h(x)) dx.$$

350 Using (3.10) and (3.11), we then derive the semi-discrete areal productivity from (3.8).  
 351 Note that  $V = h_0 L$ ,  $X(h_0)$  and  $\bar{\mu}_{N_z}(h, h_0)$  explicitly depend on the average depth  
 352  $h_0 > 0$ . To treat this parameter, we introduce an additional state variable  $y$ , such  
 353 that  $y' = 0$  and  $y = h_0$ . This state variable plays the role of  $h_0$ .

354 We are now in a position to state the optimal control problem. In the non-constant  
 355 volume case, we are looking for admissible controls  $h \in L^\infty([0, L]; \mathbb{R})$ ,  $h > -y$  and  
 356  $y > 0$  over a fixed length  $L > 0$ , which maximize the semi-discrete areal productivity.  
 357 In view of (3.8), the OCP reads as

$$\begin{aligned}
 & \max_{\substack{h \in L^\infty([0, L]; \mathbb{R}) \\ h > -y, y > 0}} \Pi_{N_z}(h) := \sum_{i=1}^{N_z} \int_0^L \frac{\mu(C_i, I_i(y+h))}{LN_z} (y+h) X(y) dx, \\
 & (P2) \quad C_i' = \frac{\beta(I_i(h+y)) - \alpha(I_i(h+y)) C_i}{Q_0} (h+y), \\
 & \quad C_i(0) = C_i(L), \quad \forall i = 1, \dots, N_z, \\
 & \quad v' = h, \\
 & \quad v(0) = 0, \quad v(L) = 0, \\
 & \quad y' = 0.
 \end{aligned}$$

359 Here again, we use formula (2.14) for  $\mu$  and  $h$  is the control variable. Moreover  
 360  $(C_i, v, y)$  are the state variables, and  $X$  is given by (3.10). The Hamiltonian denoted

361 by  $\tilde{H}$  for the OCP (P2) is given by

$$362 \quad \begin{aligned} \tilde{H}(C_i, v, y, p_{C_i}, p_v, p_y, p_0, h) &= \sum_{i=1}^{N_z} p_{C_i} \frac{\beta(I_i(h+y)) - \alpha(I_i(h+y)) C_i}{Q_0} (h+y) \\ &+ p_v h + p_y \cdot 0 + p_0 \sum_{i=1}^{N_z} \frac{\mu(C_i, I_i(y+h))}{LN_z} (h+y) X(y). \end{aligned}$$

363 Here,  $(p_{C_i}, p_v, p_y)$  denote the co-states of  $(C_i, v, y)$  respectively, and  $p_0$  is a real num-  
 364 ber. Suppose that  $h^* \in L^\infty([0, L]; \mathbb{R})$ ,  $h^* > -y^*$  is a maximizer, and  $(C_i^*, v^*, y^*)$  are  
 365 the corresponding solutions of the problem (P2). Using once again the weak maximum  
 366 principle, there exist absolutely continuous functions  $p_{C_i}^* : [0, L] \rightarrow \mathbb{R}$ ,  $p_v^* : [0, L] \rightarrow \mathbb{R}$ ,  
 367  $p_y^* : [0, L] \rightarrow \mathbb{R}$  and a real number  $p_0^* \leq 0$ , such that for almost every  $x \in [0, L]$ , the  
 368 extremals  $(C_i^*, v^*, y^*, p_{C_i}^*, p_v^*, p_y^*, p_0^*, h^*)$  satisfy the optimality system  
 (3.12)

$$\begin{aligned} v' &= \frac{\partial \tilde{H}}{\partial p_v} = h, \quad p_v' = -\frac{\partial \tilde{H}}{\partial v} = 0, \quad y' = \frac{\partial \tilde{H}}{\partial p_y} = 0, \\ p_{C_i}' &= -\frac{\partial \tilde{H}}{\partial C_i} = p_{C_i} \frac{\alpha(I_i(h+y))}{Q_0} (h+y) + p_0 \frac{\gamma(I_i(h+y))}{LN_z} (h+y) X(y), \\ C_i' &= \frac{\partial \tilde{H}}{\partial p_{C_i}} = \frac{\beta(I_i(h+y)) - \alpha(I_i(h+y)) C_i}{Q_0} (h+y), \\ p_y' &= -\frac{\partial \tilde{H}}{\partial y} = -\sum_{i=1}^{N_z} p_{C_i} \frac{\beta'(I_i(h+y)) - \alpha'(I_i(h+y)) C_i}{Q_0} (h+y) \partial_y I_i(h+y) \\ &\quad - \sum_{i=1}^{N_z} p_{C_i} \frac{\beta(I_i(h+y)) - \alpha(I_i(h+y)) C_i}{Q_0} \\ &\quad - p_0 \sum_{i=1}^{N_z} \frac{\zeta'(I_i(h+y)) - \gamma'(I_i(h+y)) C_i}{LN_z} (h+y) X(y) \partial_y I_i(h+y) \\ &\quad - p_0 \sum_{i=1}^{N_z} \frac{\zeta(I_i(h+y)) - \gamma(I_i(h+y)) C_i}{LN_z} (X(y) + (h+y) X'(y)) - p_v, \\ 0 &= \frac{\partial \tilde{H}}{\partial h} = \sum_{i=1}^{N_z} p_{C_i} \frac{\beta'(I_i(h+y)) - \alpha'(I_i(h+y)) C_i}{Q_0} (h+y) \partial_h I_i(h+y) \\ &\quad + \sum_{i=1}^{N_z} p_{C_i} \frac{\beta(I_i(h+y)) - \alpha(I_i(h+y)) C_i}{Q_0} \\ &\quad + p_0 \sum_{i=1}^{N_z} \frac{\zeta'(I_i(h+y)) - \gamma'(I_i(h+y)) C_i}{LN_z} (h+y) X(y) \partial_h I_i(h+y) \\ &\quad + p_0 \sum_{i=1}^{N_z} \frac{\zeta(I_i(h+y)) - \gamma(I_i(h+y)) C_i}{LN_z} X(y) + p_v. \end{aligned}$$

370 LEMMA 3.7. *The extremals  $(C_i^*, v^*, y^*, p_{C_i}^*, p_v^*, p_y^*, p_0^*, h^*)$  which satisfies (3.12) is*  
 371 *normal.*

372 *Proof.* We follow the same reasoning as in the proof of Lemma 3.2. Suppose that  
 373  $p_0^* = 0$ , and substitute it into the system (3.12), the ODE associated with  $p_{C_i}^*$  becomes

$$374 \quad p_{C_i}^*{}' = p_{C_i}^* \frac{\alpha(I_i(h^* + y^*))}{Q_0} (h^* + y^*), \quad p_{C_i}^*(0) = p_{C_i}^*(L), \quad \forall i = 1, \dots, N_z.$$

375 Since  $y^* = h_0 > 0$  and the function  $h^* > y^*$ , we have  $\frac{\alpha(I_i(h^* + y^*))}{Q_0} (h^* + y^*) > 0$ . This  
 376 implies that  $p_{C_i}^* = 0$ . Substituting then  $p_{C_i}^* = 0$  and  $p_0^* = 0$  into the last equation  
 377 in the system (3.12), we obtain that  $p_v^* = 0$ , which then implies that  $p_y^*{}' = 0$ . As  
 378  $p_y$  is the co-state associated with the constant  $y = h_0$ , we have  $p_y^*(0) = p_y^*(L) = 0$ ,  
 379 meaning that  $p_y^*$  equals also constantly to 0. Thus,  $p_{C_i}^*$ ,  $p_v^*$ ,  $p_y^*$  are identically 0 on  
 380  $[0, L]$ ; which concludes the proof.  $\square$

381 Based on Lemma 3.7, we can normalize the co-states such that  $p_0 = -1$ . However,  
 382 unlike Theorem 3.3, the flat topography does not satisfy the optimality system (3.12).

383 **THEOREM 3.8.** *Given  $h_0 > 0$ , let  $h^f := 0$ ,  $y^f := h_0$ ,  $p_0 = -1$  and assume that*  
 384  *$I_s \in (I_-, I_+)$ . Then there does not exist a triple  $(C_i^f, p_y^f, p_v^f)$  that satisfies the last*  
 385 *three equations in the optimality system (3.12).*

386 *Proof.* Assuming that there exists such a triple, we start by solving the ODE  
 387 associated with  $C_i^f$  in (3.12). From (3.2), (3.7) and (3.10), we obtain

$$388 \quad (3.13) \quad I_i(h + y) = I_s \exp\left(-\frac{Y_{\text{opt}}}{y} \frac{i - \frac{1}{2}}{N_z} (h + y)\right),$$

389 where  $Y_{\text{opt}}$  is defined in (3.10). Substituting the values of  $h^f$  and  $y^f$  into (3.13),  
 390 we find that  $I_i(h^f + y^f) = I_i(h_0) = I_s \exp(-Y_{\text{opt}} \frac{i - \frac{1}{2}}{N_z})$ , which is a constant with  
 391 respect to  $h_0$ . A similar analysis to that of in the proof of Theorem 3.3 shows that  
 392  $C_i^f = \beta(I_i(h_0))/\alpha(I_i(h_0))$ , which is also a constant. Furthermore, differentiating  
 393  $I_i(h + y)$  with respect to  $y$  gives  $\partial_y I_i(h + y) = I_i(h + y) \cdot \frac{Y_{\text{opt}}}{y^2} \cdot \frac{i - \frac{1}{2}}{N_z} h$ . Setting  $h = h^f$   
 394 in this expression, we get  $\partial_y I_i(h^f + y) = \partial_y I_i(0 + y) = 0$ . Substituting all these  
 395 expression into the last two equations in (3.12), we get

$$396 \quad (p_y^f)' = \frac{X(h_0) + h_0 X'(h_0)}{LN_z} \sum_{i=1}^{N_z} \mu_s(I_i(h_0)) - p_v^f, \quad p_v^f = \frac{X(h_0)}{LN_z} \sum_{i=1}^{N_z} \mu_s(I_i(h_0)).$$

397 This implies that  $(p_y^f)' = -\frac{Y_{\text{opt}}}{LN_z h_0 \varepsilon_0} \sum_{i=1}^{N_z} \mu_s(I_i(h_0))$ , so that, using (3.10), we get  
 398  $X'(h_0) = -\frac{Y_{\text{opt}}}{h_0^2 \varepsilon_0}$ . Moreover,  $I_i(h_0) \in [I_{N_z}(h_0), I_1(h_0)] \subset (I_-, I_s) \subset (I_-, I_+)$ , hence  
 399  $\mu_s(I_i(h_0)) > 0$  for  $i \in \{1, \dots, N_z\}$ . We deduce that  $(p_y^f)' < 0$ . As  $p_y^f(0) = p_y^f(L) = 0$ ,  
 400 we find a contradiction, which concludes the proof.  $\square$

401 **Remark 3.9.** Note that the coefficient  $h_0$  considered in Theorem 3.8 must satisfy  
 402  $h_c \leq h_0$  to guarantee that the system remains in a subcritical regime (see Remark 2.1).

403 **4. Numerical Experiments.** In this section, we show some optimal topogra-  
 404phies obtained in the various previous frameworks.

405 **4.1. Numerical Methods.** To solve our optimization problem numerically, we  
 406 introduce a supplementary space discretization with respect to  $x$ . In this way, let us  
 407 take a space increment  $\Delta x$ , set  $N_x = [L/\Delta x]$  and  $x^{n_x} = n_x \Delta x$  for  $n_x = 0, \dots, N_x$ .

TABLE 1  
Parameter values for Han Model

$k_r$	$6.8 \cdot 10^{-3}$	$s^{-1}$
$k_d$	$2.99 \cdot 10^{-4}$	-
$\tau$	0.25	s
$\sigma$	0.047	$m^2 \mu\text{mol}^{-1}$
$k$	$8.7 \cdot 10^{-6}$	-
$R$	$1.389 \cdot 10^{-7}$	$s^{-1}$

408 We use Heun’s method to compute  $(C_i)_{i=1}^{N_z}$  via (3.4). Following a first-discretize-  
 409 then-optimize strategy, we get that the co-states  $(p_i^C)_{i=1}^{N_z}$  are also computed by a  
 410 Heun’s type scheme. Note that this scheme is still explicit, since it solves a backward  
 411 dynamics starting from  $p_i(L) = 0$ . The optimization is then achieved by a standard  
 412 gradient method using (3.4) and (3.12), where the stopping criterion involves both the  
 413 magnitude of the gradient and the constraint  $h \geq h_c$ , see Remark 2.1. The numerical  
 414 tests are performed by *MATLAB R2020a* [34].

415 **4.2. Parameter setting.** We now detail the parameters used in our simulations.

416 **4.2.1. Parameterization.** In our tests, we parameterize  $h$  by means of a trun-  
 417 cated Fourier series. More precisely, the water depth reads:

$$418 \quad h(x; \mathbf{a}) + h_0 = h_0 + \sum_{n=1}^N a_n \sin(2n\pi \frac{x}{L}),$$

419 with  $\mathbf{a} = (a_1, \dots, a_N)$ . This parameterization is motivated by three reasons.

- 420 • The regularity of the topography is controlled by the order of truncation  $N$ .  
 421 As an example, limit situations where  $N \rightarrow +\infty$  are not considered in what  
 422 follows. This framework is consistent with the hydrodynamic regime under  
 423 consideration, where the solutions of the Saint-Venant equations are smooth.
- 424 • The constraint  $h(0; \mathbf{a}) = h(L; \mathbf{a})$ , is preserved, which fits the toric shape of  
 425 the raceway pond.
- 426 • The water depth has the form  $h_0 + h$ , as assumed in Section 3.3.

427 From (2.2) and (2.4),  $u$  and  $z_b$  also read as functions of  $\mathbf{a}$ . Once the vector  $\mathbf{a}$  that  
 428 maximizes  $\bar{\mu}_{N_z}$  is determined, we then find the optimal topography of our system.

429 **4.2.2. Parameter for the models.** The spatial increment is set to  $\Delta x = 0.01$  m  
 430 so that the convergence of the numerical scheme has been ensured, and we set the  
 431 raceway length  $L = 100$  m, the averaged discharge  $Q_0 = 0.04 \text{ m}^2 \text{ s}^{-1}$ , the average  
 432 depth (in the constant volume case)  $h_0 = h(0; \mathbf{a}) = 0.4$  m and  $z_b(0) = -0.4$  m to stay  
 433 in standard ranges for a raceway [14]. The free-fall acceleration  $g = 9.81 \text{ m s}^{-2}$ . The  
 434 values of all parameters in Han’s model are taken from [16] and given in Table 1.

435 In order to determinate the light extinction  $\varepsilon$ , two cases must be considered:

- 436 • constant volume: we assume that only 1% of light can be captured by the cells  
 437 at the average depth of the raceway, meaning that  $I_- = 0.01 I_s$ , we choose  
 438  $I_s = 2000 \mu\text{mol m}^{-2} \text{ s}^{-1}$  which approximates the maximum light intensity,  
 439 e.g., at summer in the south of France. Then  $\varepsilon$  can be computed by  $\varepsilon =$   
 440  $(1/h_0) \ln(I_s/I_-)$ .
- 441 • non-constant volume: in the case,  $h_0$  is also a parameter to be optimized.  
 442 We take from [22] the specific light extinction coefficient of the microalgae

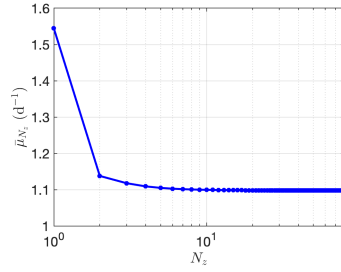


FIG. 3. Values of the functional  $\bar{\mu}_{N_z}$  for  $N_z = [1, 80]$ .

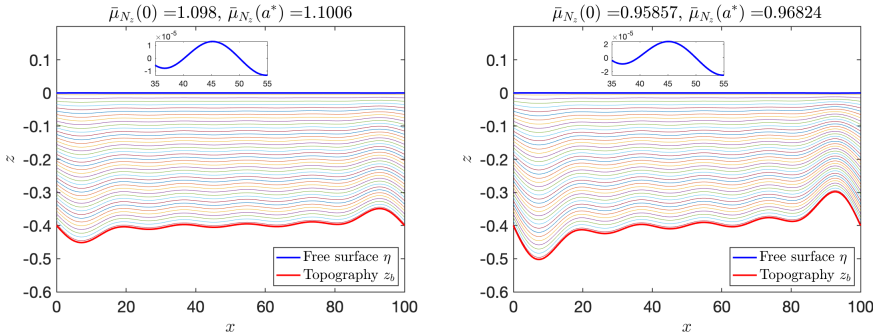


FIG. 4. Optimal topography for  $C_0 = 0.1$  (left) and  $C_0 = 0.9$  (right). The red thick line represents the topography  $z_b$ , the blue thick line represents the free surface  $\eta$ , and all the other curves between represent the different trajectories.  $\bar{\mu}_{N_z}(0)$ : flat topography,  $\bar{\mu}_{N_z}(a^*)$ : optimal topography.

443 species  $\varepsilon_0 = 0.2 \text{ m}^2 \cdot \text{g}$  and the background turbidity  $\varepsilon_1 = 10 \text{ m}^{-1}$ .

444 **4.3. Numerical results.** We test the influence of various parameters on opti-  
 445 mal topographies. In all of our experiments, we always observe that the obtained  
 446 topographies satisfy  $\min_{x \in [0, L]} h(x; \mathbf{a}) > h_c$ .

447 **4.3.1. Influence of vertical discretization.** The first test consists in studying  
 448 the influence of the vertical discretization parameter  $N_z$ . We choose  $N = 5$ ,  $C_0 = 0.1$   
 449 and consider 100 random values  $a$ . Note that the choice of  $a$  should respect the  
 450 subcritical condition. Let  $N_z$  vary from 1 to 80, and we compute the average value of  
 451  $\bar{\mu}_{N_z}$  for each  $N_z$ . The results are shown in Fig. 3. We observe numerical convergence  
 452 when  $N_z$  grows, showing the convergence towards the continuous model in space. In  
 453 view of these results, we take hereafter  $N_z = 40$ .

454 **4.3.2. Influence of the initial condition.** Here, we study the influence of the  
 455 initial condition  $C_0$  on the optimal shape of the raceway pond. We set the numeri-  
 456 cal tolerance to  $\text{Tol} = 10^{-10}$ , and consider the order of truncation  $N = 5$ . As for  
 457 the initial guess, we consider the flat topography, meaning that  $\mathbf{a}$  is set to 0. We  
 458 compare the optimal topographies obtained with  $C_0 = 0.1$  and with  $C_0 = 0.9$ . The  
 459 result is shown in Fig. 4. This test confirms Remark 3.5, since we obtain non-trivial  
 460 topographies which slightly enhance the algal average growth rate. Moreover, a slight  
 461 difference between the two optimal topographies is observed. We have observed that  
 462 this difference remains when the spatial increment  $\Delta x$  goes to zero. Although it is  
 463 difficult to observe in Fig. 4, the free surface is not equal to zero, as can be seen for

TABLE 2  
Behaviour of the objective function for various orders of truncation  $N$ .

$N$	Iter	$\bar{\mu}_{N_z}(\mathbf{a}^*)(d^{-1})$	$\log_{10}(\ \nabla \bar{\mu}_{N_z}(\mathbf{a}^*)\ )$	$\lambda_{max}(\text{Hess } \bar{\mu}_{N_z}(\mathbf{a}^*))$
0	0	1.098	—	—
5	16	1.1006	-10.208017	-6.1400
10	17	1.1013	-10.240885	-5.9141
15	17	1.1016	-10.258798	-5.9074
20	18	1.1018	-10.269413	-5.9032

464  $x \in [35, 55]$ .

465 **4.3.3. Influence of Fourier series truncation.** The next test is dedicated to  
 466 the study of the influence of the order of truncation  $N$  used to parameterize the water  
 467 depth  $h$ . Set  $N = [0, 5, 10, 15, 20]$ ,  $C_0 = 0.1$  and keep all the other parameters as in the  
 468 previous section. Table 2 shows the optimal value of  $\bar{\mu}_{N_z}(\mathbf{a}^*)$  and the corresponding  
 469 maximum eigenvalue of the Hessian  $\lambda_{max}(\text{Hess } \bar{\mu}_{N_z}(\mathbf{a}^*))$  for various values of  $N$ .

470 The result shows a slight increase in the optimal value of  $\bar{\mu}_{N_z}(\mathbf{a}^*)$  when  $N$  becomes  
 471 larger. However, the corresponding values of  $\bar{\mu}_{N_z}(\mathbf{a}^*)$  remain close to the one associ-  
 472 ated with a flat topography. Furthermore, the maximum spectrum  $\lambda_{max}(\text{Hess } \bar{\mu}_{N_z}(\mathbf{a}^*))$   
 473 is always negative, which confirms that local maximizers are obtained.

474 **4.3.4. Optimal topographies in periodic case.** We study the optimal to-  
 475 pographies in the constant volume case where the photoinhibition state  $C$  is periodic.  
 476 In our discrete setting, the Hessian operator is actually of the form  $\text{Hess } \bar{\mu}_{N_z}(h^f) =$   
 477  $\lambda Id_N$  with  $Id_N$  the identity matrix of size  $N$ . We observe that  $\lambda < 0$ , which confirms  
 478 that the flat topography is a local maximizer. A precise computation of  $\lambda$  together  
 479 with some remarks about its sign can be found in Appendix B.

480 In order to test whether this local maximizer is global, we run the optimization  
 481 procedure with random admissible topographies. We observe that the procedure  
 482 always converges to a flat topography (i.e.  $\mathbf{a}^* = a_f$ ). This leads us to conjecture that  
 483 the flat topography corresponds to the global maximum for the average growth rate.  
 484 As for the variable volume case, let us set  $N = 5$  (i.e.  $\tilde{\mathbf{a}} \in \mathbb{R}^6$ ) and  $h_0 = 0.4$  as an  
 485 initial guess of the average depth. We observe that the optimization stops due to the  
 486 presence of the physical constraint  $h_c$ . However, a smaller depth increases the areal  
 487 productivity, in some cases more than twice the initial areal productivity.

488 **4.3.5. Simulation with paddle wheel.** In this paragraph, we consider the full  
 489 raceway pond, where the mixing induced by the paddle wheel is also considered. More  
 490 precisely, we simulate several laps with a paddle wheel that mixes up the algae after  
 491 each lap. The turbulent mixing of the paddle wheel is modeled by a permutation  
 492 matrix  $P$  which rearranges the trajectories at each lap. In our test,  $P$  is chosen as an  
 493 anti-diagonal matrix with entries equal to one. This choice actually corresponds to  
 494 an optimum and, as shown in [4], where other choices are also investigated.

495 The permutation matrix  $P$  corresponds to the permutation  $\pi = (1 N_z)(2 N_z -$   
 496  $1)(3 N_z - 2) \dots$ , where we use the standard notation of cycles in the symmetric  
 497 group. Note that  $\pi$  is of order two. The photoinhibition state  $C$  is then set to be  
 498 2-periodic (i.e.,  $C^1(0) = PC^2(L)$ , where  $C^1$  and  $C^2$  correspond to the photoinhibition  
 499 state during the first and second lap, respectively). The details of the optimization  
 500 procedure are given in Appendix A.

501 We choose a truncation of order  $N = 5$  in the Fourier series. The initial guess  $a$  is

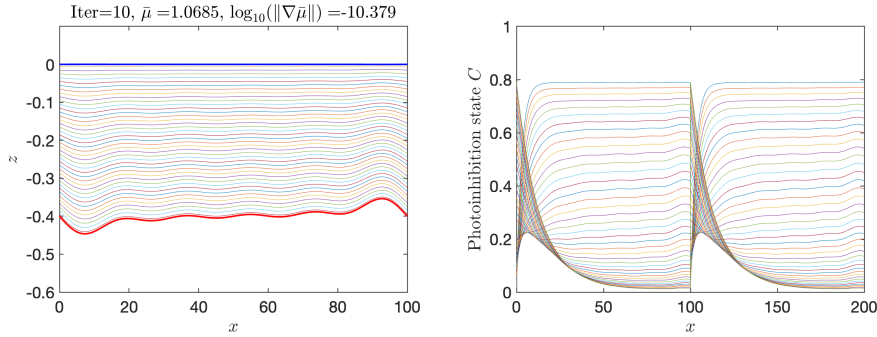


FIG. 5. *Optimal topography (left) and evolution of the photo-inhibition state  $C$  (right) over two laps.*

502 set to zero. Fig. 5 presents the shape of the optimal topography and the evolution of  
 503 the photoinhibition state  $C$  over two laps. The resulting optimal topography in this  
 504 case is not flat. However, the increase in the optimal value of the objective function  
 505  $\bar{\mu}_{N_z}$  compared to a flat topography with and without permutation are 0.217% and  
 506 0.265%, respectively, meaning that the increase remains small. On the other hand,  
 507 we observe that the state  $C$  is actually periodic for each lap. This result is actually  
 508 proved for arbitrary  $P$  in [4] in the case of a flat topography. This justifies that the  
 509 optimization strategy only need to focus on one lap of the raceway (whatever the  
 510 permutation), and leaves the door open to the optimization of such mixing strategies.  
 511 We refer to [3, 5] for more details on optimal mixing strategies.

512 **5. Conclusions and future works.** A flat topography cancels the average algal  
 513 growth rate gradient when  $C$  is assumed to be periodic along the laminar parts of  
 514 the raceway. This is further confirmed by our numerical tests, in which maximum  
 515 productivity is obtained for a flat topography. However, considering a more complete  
 516 framework without periodicity and including a mixing device gives rise to an optimal  
 517 non-flat topography with a slight gain of the average growth rate. It is not clear  
 518 whether the difficulty in designing such a pattern could be compensated for by the  
 519 increase in the process productivity.

520 These results may no longer hold if the hydrodynamic regime is turbulent along  
 521 the entire raceway. In such a case, the increase in the algal productivity may compen-  
 522 sate for the higher energetic cost of mixing. However, without the laminar assumption,  
 523 the problem becomes challenging, and much work remains to be done in this direction.

524 **Acknowledgements.** We are very grateful to Emmanuel Trélat (Laboratoire  
 525 Jacques-Louis Lions, Sorbonne Université, Paris) for the helpful discussions we have  
 526 had on this topic. We thank the editors and the anonymous referees for their valuable  
 527 and constructive comments, which greatly improved the quality of this paper.

528

#### REFERENCES

- 529 [1] O. BERNARD, A.-C. BOULANGER, M.-O. BRISTEAU, AND J. SAINTE-MARIE, *A 2D model for*  
 530 *hydrodynamics and biology coupling applied to algae growth simulations*, ESAIM: Mathe-  
 531 *matical Modelling and Numerical Analysis*, 47 (2013), pp. 1387–1412.  
 532 [2] O. BERNARD AND L.-D. LU, *Optimal optical conditions for microalgal production in photo-*  
 533 *bioreactors*, *Journal of Process Control*, 112 (2022), pp. 69–77.  
 534 [3] O. BERNARD, L.-D. LU, AND J. SALOMON, *Mixing strategies combined with shape design to*  
 535 *enhance productivity of a raceway pond*, in 16th IFAC Symposium on Advanced Control

- of Chemical Processes ADCHEM 2021, vol. 54, 2021, pp. 281–286.
- [4] O. BERNARD, L.-D. LU, AND J. SALOMON, *Optimizing microalgal productivity in raceway ponds through a controlled mixing device*, in 2021 American Control Conference (ACC), IEEE, 2021, pp. 640–645.
- [5] O. BERNARD, L.-D. LU, AND J. SALOMON, *Optimal periodic resource allocation in reactive dynamical systems: Application to microalgal production*, International Journal Of Robust And Nonlinear Control, (2022).
- [6] O. BERNARD, F. MAIRET, AND B. CHACHUAT, *Modelling of microalgae culture systems with applications to control and optimization*, Microalgae Biotechnology, 153 (2015).
- [7] A. BOUHARGUANE AND B. MOHAMMADI, *Minimization principles for the evolution of a soft sea bed interacting with a shallow*, International Journal of Computational Fluid Dynamics, 26 (2012), pp. 163–172.
- [8] F. CASAGLI, G. ZUCCARO, O. BERNARD, J.-P. STEYER, AND E. FICARA, *Alba: A comprehensive growth model to optimize algae-bacteria wastewater treatment in raceway ponds*, Water Research, 190 (2021), p. 116734.
- [9] D. CHIARAMONTI, M. PRUSSI, D. CASINI, M. TREDICI, L. RODOLFI, N. BASSI, G. ZITTELLI, AND P. BONDIOLI, *Review of energy balance in raceway ponds for microalgae cultivation: Re-thinking a traditional system is possible*, Applied Energy, 102 (2013), pp. 101–111.
- [10] P.-H. COCQUET, S. RIFFO, AND J. SALOMON, *Optimization of bathymetry for long waves with small amplitude*, SIAM Journal on Control and Optimization, 59 (2021), pp. 4429–4456.
- [11] R. DE-LUCA, F. BEZZO, Q. BÉCHET, AND O. BERNARD, *Exploiting meteorological forecasts for the optimal operation of algal ponds*, Journal of Process Control, 55 (2017), pp. 55–65.
- [12] D. DEMORY, C. COMBE, P. HARTMANN, A. TALEC, E. PRUVOST, R. HAMOUDA, F. SOUILLÉ, P.-O. LAMARE, M.-O. BRISTEAU, J. SAINTE-MARIE, S. RABOUILLE, F. MAIRET, A. SCIANDRA, AND O. BERNARD, *How do microalgae perceive light in a high-rate pond? towards more realistic lagrangian experiments*, The Royal Society, (2018).
- [13] P. EILERS AND J. PEETERS, *Dynamic behaviour of a model for photosynthesis and photoinhibition*, Ecological Modelling, 69 (1993), pp. 113 – 133.
- [14] T. B. F. RAYEN AND P. DOMINIQUE, *Optimization of a raceway pond system for wastewater treatment: a review*, Critical Reviews in Biotechnology, 39 (2019), pp. 422–435.
- [15] J.-F. GERBEAU AND B. PERTHAME, *Derivation of viscous saint-venant system for laminar shallow water; numerical validation*, Discrete & Continuous Dynamical Systems - B, 1 (2001), pp. 89–102.
- [16] J. GRENIER, F. LOPES, H. BONNEFOND, AND O. BERNARD, *Worldwide perspectives of rotating algal biofilm up-scaling*. Submitted, 2020.
- [17] F. GROGNARD, A. AKHMETZHANOV, AND O. BERNARD, *Optimal strategies for biomass productivity maximization in a photobioreactor using natural light*, Automatica, 50 (2014), pp. 359–368.
- [18] B.-P. HAN., *A mechanistic model of algal photoinhibition induced by photodamage to photosystem-II*, Journal of theoretical biology, 214 (2002), pp. 519–527.
- [19] R. HREIZ, B. SIALVE, J. MORCHAIN, R. ESCUDIÉ, J.-P. STEYER, AND P. GUIRAUD, *Experimental and numerical investigation of hydrodynamics in raceway reactors used for algaculture*, Chemical Engineering Journal, 250 (2014), pp. 230–239.
- [20] C. INOSTROZA, A. SOLIMENO, J. GARCÍA, J. FERNÁNDEZ-SEVILLA, AND F. ACIÉN, *Improvement of real-scale raceway bioreactors for microalgae production using computational fluid dynamics (CFD)*, Algal Research, 54 (2021), p. 102207.
- [21] P.-O. LAMARE, N. AGUILLON, J. SAINTE-MARIE, J. GRENIER, H. BONNEFOND, AND O. BERNARD, *Gradient-based optimization of a rotating algal biofilm process*, Automatica, 105 (2019), pp. 80–88.
- [22] C. MARTÍNEZ, F. MAIRET, AND O. BERNARD, *Theory of turbid microalgae cultures*, Journal of Theoretical Biology, 456 (2018), pp. 190–200.
- [23] P. MASCI, F. GROGNARD, AND O. BERNARD, *Microalgal biomass surface productivity optimization based on a photobioreactor model*, IFAC Proceedings Volumes, 43 (2010), pp. 180–185.
- [24] J. MASOJÍDEK, Š. PAPÁČEK, M. SERGEJEVOVÁ, V. JIRKA, J. ČERVENÝ, J. KUNC, J. KOREČKO, O. VERBOVIKOVA, J. KOPECKÝ, D. ŠTYS, AND G. TORZILLO, *A closed solar photobioreactor for cultivation of microalgae under supra-high irradiance: Basic design and performance*, Journal of Applied Phycology, 15 (2003), pp. 239–248.
- [25] J. MENDOZA, M. GRANADOS, I. DE GODOS, F. ACIÉN, E. MOLINA, C. BANKS, AND S. HEAVEN, *Fluid-dynamic characterization of real-scale raceway reactors for microalgae production*, Biomass and Bioenergy, 54 (2013), pp. 267–275.
- [26] V. MICHEL-DANSAC, C. BERTHON, S. CLAIN, AND F. FOUCHER, *A well-balanced scheme for the shallow-water equations with topography*, Computers and Mathematics with Applications,

- 598 72 (2016), pp. 586–593.
- 599 [27] B. MOHAMMADI AND A. BOUHARGUANE, *Optimal dynamics of soft shapes in shallow waters*,  
 600 *Computers and Fluids*, 40 (2011), pp. 291–298.
- 601 [28] R. MUÑOZ-TAMAYO, F. MAIRET, AND O. BERNARD, *Optimizing microalgal production in race-*  
 602 *way systems*, *Biotechnology progress*, 29 (2013), pp. 543–552.
- 603 [29] G. OLIVIERI, L. GARGIULO, P. LETTIERI, L. MAZZEI, P. SALATINO, AND A. MARZOCHELLA,  
 604 *Photobioreactors for microalgal cultures: A lagrangian model coupling hydrodynamics and*  
 605 *kinetics*, *Biotechnology progress*, 31 (2015), pp. 1259–1272.
- 606 [30] S. PAPACEK, J. JABLONSKY, AND K. PETERA, *Advanced integration of fluid dynamics and*  
 607 *photosynthetic reaction kinetics for microalgae culture systems*, *BMC systems biology*, 12  
 608 (2018), pp. 1–12.
- 609 [31] C. POSTEN AND S. CHEN, eds., *Microalgae Biotechnology*, 153, Springer, 1 ed., 2016.
- 610 [32] M. PRUSSI, M. BUFFI, D. CASINI, D. CHIARAMONTI, F. MARTELLI, M. CARNEVALE, M. TREDICI,  
 611 AND L. RODOLFI, *Experimental and numerical investigations of mixing in raceway ponds*  
 612 *for algae cultivation*, *Biomass and bioenergy*, 67 (2014), pp. 390–400.
- 613 [33] M. V. SOLODOV, *Constraint Qualifications*, John Wiley & Sons, Ltd, 2011.
- 614 [34] THE MATHWORKS INC., *Matlab version: 9.8.0 (r2020a)*, 2020.
- 615 [35] E. TRÉLAT, *Control in Finite and Infinite Dimension*, Springer Singapore, 1 ed., 2024.
- 616 [36] A. VAN DONGEREN, N. PLANT, A. COHEN, D. ROELVINK, M. HALLER, AND P. CATALÁN, *Beach*  
 617 *wizard: Nearshore bathymetry estimation through assimilation of model computations and*  
 618 *remote observations*, *Coastal Engineering*, 55 (2008), pp. 1016–1027.
- 619 [37] R. WIJFFELS AND M. BARBOSA, *An outlook on microalgal biofuels*, *Science*, 329 (2010), pp. 796–  
 620 799.
- 621 [38] S. YOO, S.-K. OH, AND J. LEE, *Design of experiments and sensitivity analysis for microalgal*  
 622 *bioreactor systems*, in 22nd European Symposium on Computer Aided Process Engineering,  
 623 I. D. L. Bogle and M. Fairweather, eds., vol. 30 of *Computer Aided Chemical Engineering*,  
 624 Elsevier, 2012, pp. 722–726.

### 625 Appendix A. Two-lap system with a paddle-wheel.

626 Denote by  $P$  the permutation matrix associated with  $\pi = (1\ N_z)(2\ N_z - 1)(3\ N_z -$   
 627  $2) \dots$  (see Section 4.3.5), i.e., 1 as entries on the anti-diagonal and by  $C^1$  (resp.  $C^2$ )  
 628 the photoinhibition state for the first (resp. second) lap of the raceway. We then  
 629 assume that the state  $C$  is 2-periodic, meaning that  $C^1(0) = PC^2(L)$ . From (3.3),  
 630 we define the objective function by

$$631 \quad \frac{1}{2} \sum_{j=1}^2 \bar{\mu}_{N_z}^j(h) = \frac{1}{2} \sum_{j=1}^2 \sum_{i=1}^{N_z} \int_0^L \frac{\mu(C_i^j(x), I_i(h(x)))}{VN_z} h \, dx.$$

632 For a fixed volume  $V > 0$  and a discharge  $Q_0 > 0$ , the associated OCP reads:

$$633 \quad \begin{aligned} \max_{h \in L^\infty(0, L; \mathbb{R}), h > 0} \frac{1}{2} \sum_{j=1}^2 \bar{\mu}_{N_z}^j(h) &= \frac{1}{2} \sum_{j=1}^2 \sum_{i=1}^{N_z} \int_0^L \frac{\mu(C_i^j(x), I_i(h(x)))}{VN_z} h \, dx, \\ \text{(A.1)} \quad C_i^{j'} &= \frac{\beta(I_i(h)) - \alpha(I_i(h))C_i^j}{Q_0} h, \\ C^1(L) &= PC^2(0), \quad C^1(0) = PC^2(L), \\ v' &= h, \\ v(0) &= 0, \quad v(L) = V. \end{aligned}$$

634 Denote by  $H$  the Hamiltonian associated with this problem, which reads

$$635 \quad \begin{aligned} H(C_i^j, v, p_{C_i}^j, p_v, p_0, h) &= \sum_{j=1}^2 \sum_{i=1}^{N_z} p_{C_i}^j \left( \frac{\beta(I_i(h)) - \alpha(I_i(h))C_i^j}{Q_0} h \right) + p_v h \\ &+ p_0 \frac{1}{2} \sum_{j=1}^2 \sum_{i=1}^{N_z} \frac{\zeta(I_i(h)) - \gamma(I_i(h))C_i^j}{VN_z} h, \end{aligned}$$

636 where  $p_{C_i}^j$ ,  $p_v$  are the co-states of  $C_i$ ,  $v$ , and  $p_0$  is a real number. A similar analysis  
 637 to that of Section 3.2 gives a similar optimality system as (3.4), in which  $p_{C_i}^j$  satisfies  
 638 the conditions  $p_C^1(L) = Pp_C^2(0)$  and  $p_C^2(L) = Pp_C^1(0)$ .

639 **Appendix B. Second order conditions.** Consider second-order conditions  
 640 under the truncated Fourier parameterization. Since the Fourier modes  $(\sin(2n\pi\frac{x}{L}))_{n \in \mathbb{N}}$   
 641 are orthogonal, a direct computation gives  $\text{Hess } \bar{\mu}_{N_z}(h^f) = \lambda Id_N$  with

$$\begin{aligned} \lambda = & \frac{1}{Q_0} \sum_{i=1}^{N_z} 2p_{C_i} (\beta'(I_i(h)) - \alpha'(I_i(h))C_i) I_i'(h) + p_{C_i} (\beta'(I_i(h)) - \alpha'(I_i(h))C_i) I_i''(h)h \\ & + p_{C_i} (\beta''(I_i(h)) - \alpha''(I_i(h))C_i) I_i'(h)^2 h \\ & + \frac{p_0}{VN_z} \sum_{i=1}^{N_z} 2(\zeta'(I_i(h)) - \gamma'(I_i(h))C_i) I_i'(h) + (\zeta'(I_i(h)) - \gamma'(I_i(h))C_i) I_i''(h)h \\ & + (\zeta''(I_i(h)) - \gamma''(I_i(h))C_i) I_i'(h)^2 h. \end{aligned}$$

643 Using the definitions (2.11) and (2.15), we get  $\alpha(I) = \beta(I) + k_r$  and  $\zeta(I) = \gamma(I) - R$ .  
 644 As  $\alpha'(I) = \beta'(I)$  and  $\zeta'(I) = \gamma'(I)$ , one gets

$$\begin{aligned} \lambda = & \sum_{i=1}^{N_z} (1 - C_i) \left[ \frac{p_{C_i}}{Q_0} \left( 2\beta'(I_i(h)) I_i'(h) + \beta'(I_i(h)) I_i''(h)h + \beta''(I_i(h)) I_i'(h)^2 h \right) \right. \\ & \left. + \frac{p_0}{VN_z} \left( 2\gamma'(I_i(h)) I_i'(h) + \gamma'(I_i(h)) I_i''(h)h + \gamma''(I_i(h)) I_i'(h)^2 h \right) \right]. \end{aligned}$$

646 Furthermore, one can differentiate the closed forms of  $I(h)$ ,  $\beta(I)$  and  $\gamma(I)$  to have

$$\begin{aligned} I_i'(h) &= -\varepsilon \frac{i - \frac{1}{2}}{N_z} I_i(h), \quad I_i''(h) = \left( \varepsilon \frac{i - \frac{1}{2}}{N_z} \right)^2 I_i(h), \\ \beta''(I) &= \frac{2}{(\tau\sigma I + 1)(\tau\sigma I + 2)I} \beta'(I), \quad \gamma''(I) = -\frac{2\sigma\tau}{\tau\sigma I + 1} \gamma'(I). \end{aligned}$$

648 Inserting these analytical forms into (B.1) gives

$$\begin{aligned} \lambda = & \sum_{i=1}^{N_z} (1 - C_i) \varepsilon \frac{i - \frac{1}{2}}{N_z} I_i(h) \left[ \frac{p_{C_i} \beta'(I_i(h))}{Q_0} \left( h\varepsilon \frac{i - \frac{1}{2}}{N_z} + \frac{2h\varepsilon \frac{i - \frac{1}{2}}{N_z}}{(\tau\sigma I_i(h) + 1)(\tau\sigma I_i(h) + 2)} - 2 \right) \right. \\ & \left. + \frac{p_0 \gamma'(I_i(h))}{VN_z} \left( h\varepsilon \frac{i - \frac{1}{2}}{N_z} - \frac{2\sigma\tau h\varepsilon \frac{i - \frac{1}{2}}{N_z} I_i(h)}{\tau\sigma I_i(h) + 1} - 2 \right) \right]. \end{aligned}$$

650 Considering now the case  $h = h^f = V/L$ , one gets

$$\begin{aligned} 1 - C_i^f &= \frac{k_r}{\alpha(I_i(h^f))} > 0, \quad p_{C_i}^f = p_0 \frac{Q_0 \gamma(I_i(h^f))}{VN_z \alpha(I_i(h^f))} < 0, \\ \beta'(I) &= \frac{k_d \tau \sigma^2 I (I\sigma\tau + 2)}{(I\sigma\tau + 1)^2} > 0, \quad \gamma'(I) = \frac{k\sigma}{(I\sigma\tau + 1)^2} > 0. \end{aligned}$$

652 Hence, in the limit case, the sign in the big bracket becomes positive when  $h$  goes  
 653 to 0 and the flat topography is no longer a local maximizer for small values of  $h$   
 654 in this case. Under the assumption that the hydrodynamics is subcritical, then  $\lambda < 0$   
 655 in practice as shown in Section 4.3.3 and in Section 4.3.4.